Synthetic dyes adsorption and discoloration of a textile wastewater effluent by H₃PO₄ and H₃BO₃ activated *Thapsia transtagana* biomass

Aicha Machrouhi[a], Wafaa Boumya[a], Malika Khnifira[a], Mhamed Sadiq[a], Mohamed Abdennouri[a], Alaâeddine Elhalil[b], Hanane Tounsadi[c], Samir Qourzal[d], Noureddine Barka[a],*

[a]*Research Group in Environmental Sciences and Applied Materials (SEMA), Sultan Moulay Slimane University of Beni Mellal, FP Khouribga, B.P. 145, 25000 Khouribga, Morocco, Tel. +212 661 66 66 22; Fax: +212 523 49 03 54; emails: barkanoureddine@yahoo.fr (N. Barka), machrouhi.aicha90@gmail.com (A. Machrouhi), wafboumya@gmail.com (W. Boumya), khnifiramalak2014@gmail.com (M. Khnifina), sadiqmhamed@hotmail.com (M. Sadiq), abdennourimohamed@yahoo.fr (M. Abdennouri)*
[b]*Laboratory of Engineering, Processes and Environment (LEPE) University Hassan II, EST Casablanca, Morocco, email: elhalil.alaaeddine@gmail.com (A. Elhalil)*
[c]*Laboratoire d'Ingénierie, d'Electrochimie, de Modélisation et d'Environnement, Université Sidi Mohamed Ben Abdellah, Faculté des Sciences Dhar El Mahraz, Fès, Morocco, email: hananetounsadi@gmail.com (H. Tounsadi)*
[d]*Equipe de Catalyse et Environnement, Département de Chimie, Faculté des Sciences, Université Ibn Zohr, B.P. 8106 Cité Dakhla, Agadir, Morocco, email: samir_qourzal@yahoo.fr (S. Qourzal)*

ABSTRACT

This study aims to evaluate the adsorption properties of cationic and anionic dyes from aqueous solution and the treatment of a real textile wastewater by H_3PO_4 and H_3BO_3 activated *Thapsia transtagana* stems (TTS). Textural properties of adsorbents were observed by scanning electron microscopy with an energy dispersive X-ray. The crystalline structure was studied by X-ray diffraction and the surface chemistry was investigated by Fourier transform infrared spectroscopy, point of zero charge, and potentiometric titrations. Batch adsorption experiments were established to evaluate the influence of solution pH, adsorbent dose, contact time, temperature, and initial dyes concentration. Maximum adsorption occurred at neutral to basic pH values for cationic dyes and neutral to acid pH for anionic dyes. The adsorption capacities were higher in the case of H_3PO_4 activation compared to H_3BO_3 activation. Kinetic data were properly fitted with the pseudo-second-order model instead of pseudo-first-order model. Equilibrium uptake increased with an increase in the initial dye concentration according to Langmuir model. The process was exothermic in nature and accompanied by a decrease in entropy. Desorption studies of MB indicate that 0.1 N H_2SO_4 exhibits higher elution efficiency; 82.89% for AC-H_3PO_4 and 60.41% for AC-H_3BO_3. The optimum COD removal efficiencies in the real textile wastewater were, 69.56% and 56.20%, respectively, for H_3PO_4 and H_3BO_3 activated TTS at solution pH of 4.

Keywords: Biomass activation; Dyes removal; Textile wastewater treatment; Adsorbent regeneration

* Corresponding author.

1. Introduction

The increase of the industrial activities has given rise to a growing demand for water, while the water resources available for human activities represent only 0.03% of the global water reserves [1]. Many industries like the textile industry use dyes to color their products and thus produce polluted wastewaters. The discharge of these effluents in the receipting environment can result in several damages [2]. Dyes are visible to the human eye and therefore, a highly objectionable type of pollutant on esthetic grounds. They also interfere with the transmission of light and upset the biological metabolism processes which cause the destruction of aquatic communities present in the ecosystem [3].

A wide variety of techniques have been used for dyes removal from wastewaters including biological degradation [4], coagulation [5], membrane filtration [6], reverse osmosis [7], electrochemical oxidation [8], ozonation [9], and photocatalytic degradation [10]. Most of these technologies present major drawbacks such as long operation time, high sludge production, high cost, and eco-unfriendliness. Contrariwise, adsorption on activated biomass has emerged as a growing alternative technique for the discoloration of dye-containing effluents.

Activated carbon is widely used in adsorption processes due to its high carbon content, providing a high adsorption capacity, large surface area, and a variety of functional groups that can provide acid, basic or neutral characteristics to the material [11–13]. Many studies have been carried out to investigate the use of inexpensive biomasses to produce low-cost activated carbons using agricultural solid wastes including coffee ground [14], *Diplotaxis harra* [15], *Glebionis coronaria* L. [16], maize corncob [17], beetroot seeds [18], apricot stones [19], citrus peel [20], coconut shell [21], and tea waste [22].

In this work, the local and abundant plant *Thapsia transtagana* was utilized as a low-cost precursor for activated carbon production using one-step chemical activation by H_3PO_4 and H_3BO_3 at low temperatures (400°C–500°C). The adsorption efficiency of the prepared activated carbons for effective removal of cationic and anionic dyes was carried out as function of contact time, adsorbent dosage, initial concentration of dyes, temperature, and solution pH. Kinetic data were fitted to the pseudo-first-order and the pseudo-second-order kinetic models. Equilibrium isotherms were modeled by Langmuir and Freundlich models. Samples were characterized by several physicochemical techniques (X-ray diffraction (XRD), Fourier transform infrared (FTIR), scanning electron microscopy energy-dispersive X-ray (SEM/EDX), potentiometric titrations). Subsequently, the study of the regeneration of ACs loaded with methylene blue was carried out. Finally, to test the applicability of these activated carbons on the industrial scale, we tried to treat a textile wastewater sample from PIF-Textile factory in Berrechid City.

2. Materials and methods

2.1. Materials

All the chemicals and reagents used in this study were of analytical grade. H_3PO_4 (85%), H_3BO_3 (100%), HCl (37%), Na_2CO_3, $NaHCO_3$ (99.5%–100.5%), methyl violet, methyl orange, and indigo carmine were purchased from Sigma-Aldrich (Germany). Methylene blue was purchased from Panreac (Spain). HNO_3 (65%) was provided by Sharlau (Spain). NaOH (≥99%) from Merck (Germany). The characteristics and chemical structure of dyes are listed in Table 1. All working solutions were prepared in bidistilled water.

2.2. Preparation of activated carbon

The *Thapsia transtagana* stems (TTS) were cut into small pieces and were powdered to particles of size <125 μm using a domestic mixer. The activation was carried out using phosphoric acid and boric acid separately under conditions optimized in previous work. The TTS powder was impregnated with each activating agent at an impregnation ratio of 2 g/g. The mixtures were heated at 105°C for 24 h to remove excess moisture and then loaded in a stainless-steel vertical tubular reactor placed into a furnace. The activation was done at 400°C or 500°C for 145 min under nitrogen atmosphere. After that, the activated samples were washed with hot deionized water until neutral pH. The obtained powders were then dried at 105°C, and sieved in particles of size lower than 125 μm using a normalized sieve. The obtained adsorbents were stored in a hermetic bottle for further tests, under the names AC-H_3PO_4 and AC-H_3BO_3.

2.3. Characterization of activated carbons

The surface morphology of activated carbons was observed by SEM using TESCAN VEGA microscope (Czech Republic) equipped with an EDX detector. XRD patterns were recorded using a Bruker-axs D2-phaser diffractometer (Germany) operating at 30 kV and 10 mA with Cu Kα. FTIR spectra in a range of 4,000–400 cm⁻¹ were recorded on FTIR-2000 Perkin Elmer spectrophotometer (USA) using KBr pellets. The acidic and basic functional groups on the surface of ACs were determined quantitatively by the Boehm's titration method [23]. The pH of point of zero charge (pHpzc) was determined by Noh and Schwarz [24].
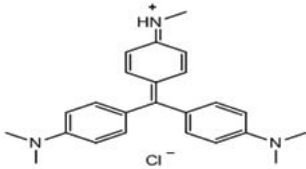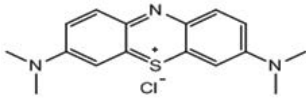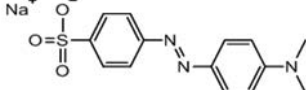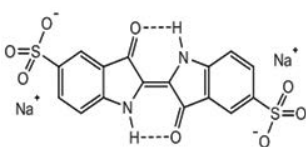
2.4. Adsorption tests

2.4.1. Adsorption/desorption and regeneration of adsorbents

Sorption experiments were done in a series of beakers containing 50 mL of the dye solution at a concentration of 500 mg/L and 50 mg of activated carbon. The mixtures were stirred at room temperature for 2 h. After each sorption experiment, samples were centrifuged at 3,000 rpm for 10 min and the residual concentration was determined using UV-vis spectrophotometer. The adsorption capacity was calculated from the difference between initial and residual concentrations.

Desorption experiment for MB were done on activated carbons initially loaded with 1 L MB solution of initial concentration of 500 mg/L at initial solution pH with the mass ratio of activated carbon of 1 g/L. After saturation, the suspension was filtered and the residual solid was contacted with distilled water and various solution of 0.1 N each (H_2SO_4, HNO_3, and NaOH) as the desorbing solution at the same operating conditions adopted in adsorption tests.

Table 1
Physical characteristics and molecular structure of dyes

Dye name	Generic name	Molecular structure	λ_{max} (nm)	M_w (g/mol)
Methyl violet (MV)	Basic violet 1		584	393.95
Methylene blue (MB)	Basic blue 9		663	319.85
Methyl orange (MO)	Acid orange 52		465	327.33
Indigo carmine (IC)	Acid blue 74		610	466.36

The percentage of MB desorbed was calculated by the following equation:

$$\% \text{ Desorption} = \frac{100 \times C_d}{q_e \times R} \qquad (1)$$

where C_d (mg/L) is the concentration of MB desorbed, q_e (mg/g) is the adsorption capacity of the adsorbent and R is the mass ratio of the activated carbon used in desorption.

2.4.2. Treatment of textile effluent

Textile wastewater (TWW) sample at the factory's discharge point was collected from a tissue dyeing mill, PIF, Berrechid, Morocco. The sample was stored at a temperature ≤5°C to avoid any change in its physicochemical characteristics before use. Treatment experiments were performed in a series of beakers containing the desired dose of ACs ranging between 0.5 and 5.0 g/L and 50 mL of the wastewater. The experiments were carried out at a constant agitation speed of 500 rpm for 3 h. The effect of pH was evaluated from 4 to 13. Color removal from TWW was estimated from the change in UV-Vis spectrum in the range of (300–900 nm). COD was analyzed by the potassium dichromate oxidation method.

The COD removal (%) was calculated by the following equation:

$$\text{COD removal}(\%) = \frac{\text{COD}_0 - \text{COD}}{\text{COD}_0} \times 100 \qquad (2)$$

where COD_0 is the initial COD concentration (mg/L), COD is the COD concentration after treatment (mg/L).

3. Results and discussion

3.1. Structural and textural properties of activated carbons

3.1.1. X ray diffraction

Fig. 1 shows the XRD patterns of activated carbons, which correspond to amorphous solids. It is clearly seen that activated carbon prepared with H_3PO_4 possessed broadband at 24° and a weak band around 38°–45° assigned to the (002) and (100) crystal planes of graphite. The weak intensity of the band around 38°–45° indicates the low crystallinity of the graphite structure. The position and width of this peak indicate that activated carbon have a coke like character with a disordered carbonaceous interlayer [25]. In addition, the XRD pattern for activated carbon prepared with H_3BO_3 indicates a more disordered structure compared to activated carbon prepared with H_3PO_4.

3.1.2. Scanning electron microscopy

SEM images of raw and TTS based activated carbons are illustrated in Fig. 2. The figure indicates that only a limited number of irregular pores are present on the surface of the raw TTS particles. The chemical activation with phosphoric acid or boric acid resulted in an increase in pore surface area and pore volume in the inner surface of activated carbons (Figs. 2b and c). From Fig. 2b, it is clear that the activated carbon treated with phosphoric acid has well-developed pores on the external surface. For AC-H_3BO_3 (Fig. 2c), it consists of irregular and heterogeneous structure with a smooth and featureless surface. This result confirms that the nature of the activation reagent influence strongly the porous structure of the resulting activated carbon.
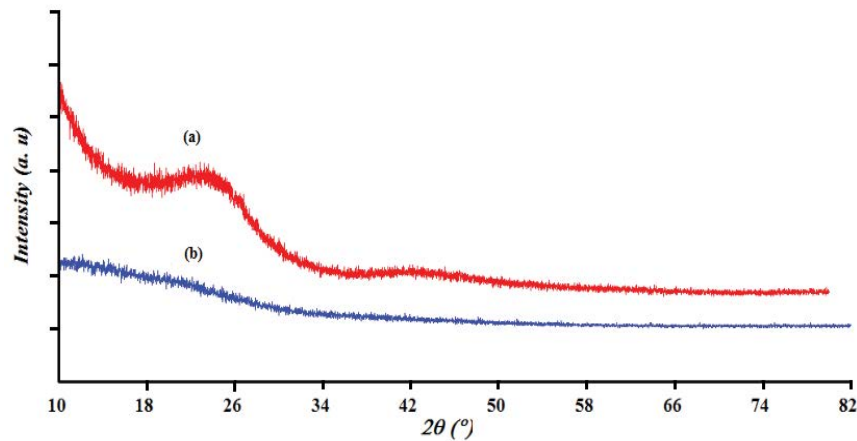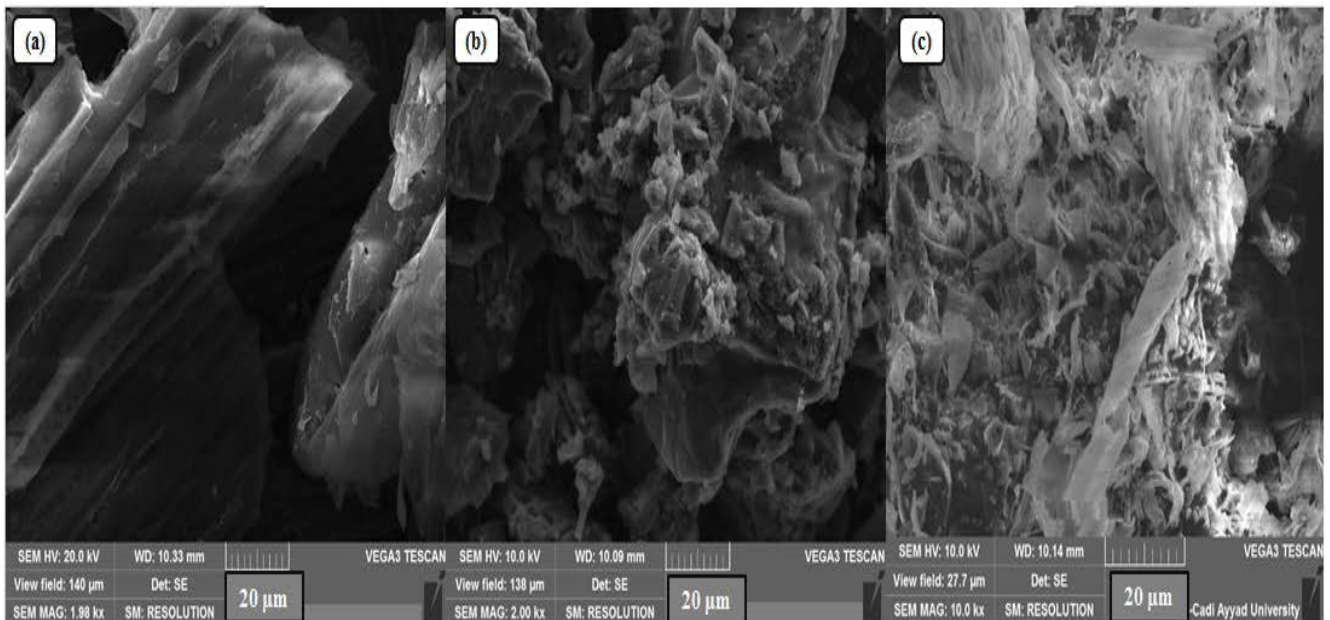
Fig. 1. XRD patterns of AC-H$_3$PO$_4$ (a) and AC-H$_3$BO$_3$ (b).

Fig. 2. SEM images of (a) precursor, (b) AC-H$_3$PO$_4$, and (c) AC-H$_3$BO$_3$.

3.1.3. Energy dispersive X-ray analysis

The results of the EDX analysis of the raw and activated TTS are given in Table 2. The table indicates that the atomic percentage of carbon and oxygen change strongly after the activation process. It was observed that the carbon percentage increased from 63.27% in the raw material to 87.44% for AC-H$_3$PO$_4$ and 76.53% for AC-H$_3$BO$_3$, while the oxygen percentage decreased from 31.45% to 12.03% for AC-H$_3$PO$_4$ and 17.73% for AC-H$_3$BO$_3$. This decrease in oxygen % was due to dehydration and decomposition of oxygen-containing groups.

3.1.4. Infrared spectroscopy

The FTIR spectra of the adsorbents are shown in Fig. 3. For the raw TTS, there is a large band between 3,700 and

Table 2
Elemental analysis of: (a) precursor, (b) AC-H$_3$PO$_4$, and (c) AC-H$_3$BO$_3$

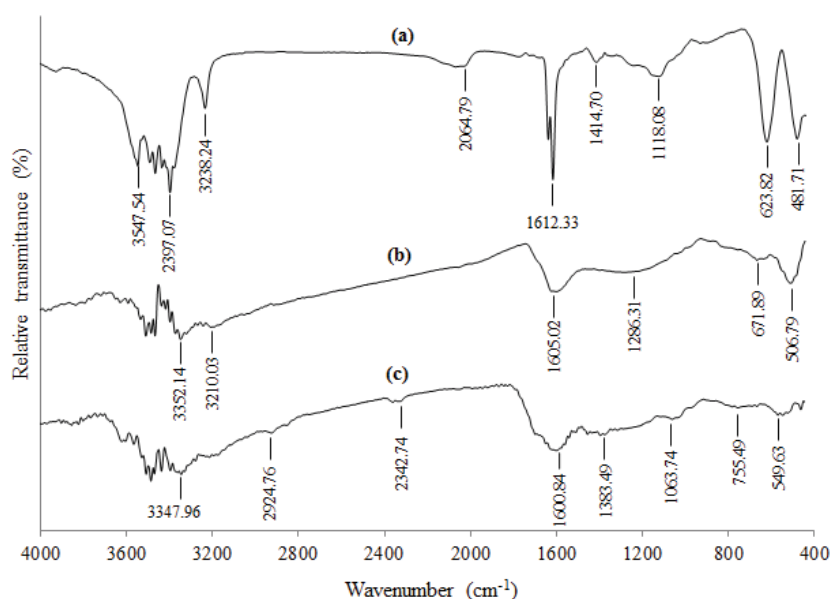| Element	Element %		
	a	b	c
C	63.27	87.44	76.53
O	31.45	12.03	17.73
P	–	0.53	–
Al	4.62	–	–
Na	0.2	–	–
Cl	0.14	–	–
K	0.12	–	–

Fig. 3. FTIR spectra of (a) precursor, (b) AC-H$_3$PO$_4$, and (c) AC-H$_3$BO$_3$.

3,200 cm^{-1} attributed to the stretching vibration of hydrogen-bended of the hydroxyl group linked in cellulose, lignin, adsorbed water, and N–H stretching [26]. The bands at 3,000–2,800 cm^{-1} are attributed to aliphatic C–H stretching vibrations in an aromatic methoxyl group, in methyl and methylene groups of side chains. The small band at 1,676 cm^{-1} is assigned to O–H bending. The spectra also indicate a band at 1,612.33 cm^{-1} characteristic of C=O stretching vibrations of ketones, aldehydes, lactones, or carboxyl groups. After chemical activation, the functional groups and surface properties of the activated carbons change from the raw biomass. Some peaks of high intensity were disappeared due to the destruction of some intermolecular bonding during activation. Most changes occurring on the AC-H$_3$PO$_4$ and AC-H$_3$BO$_3$ are reflected in the bands present between 1,400 and 1,700 cm^{-1}, which may be due to overlapping of the stretching vibration of carbon–oxygen-bended of the carboxylic group. These bands confirmed the presence of several oxygen functional groups including ketones, aldehydes, and lactones. The band corresponding to O–H stretching vibrations of the hydroxyl functional groups including hydrogen bonding, was of low intensity in ACs. This reduction in the peak intensity corresponds to the reduction in hydrogen bonding which may be due to the reaction between acid agents and precursor.

3.1.5. Boehm titration and pH of zero charge

The surface chemistry of carbon materials is basically determined by the acidity and basicity of their surface functional groups. Table 3 shows that the acidic functional groups (carboxylic, lactonic, and phenolic groups) in the case of AC-H$_3$PO$_4$ (1.451 meq/g) were higher than those of AC-H$_3$BO$_3$ (1.418 meq/g). Also, the total basic functional groups in the case of AC-H$_3$PO$_4$ (0.399 meq/g) were higher than those of AC-H$_3$BO$_3$. These results indicate that the surface chemistry of activated carbons was more developed by H$_3$PO$_4$ activation

compared to H$_3$BO$_3$ activation. Table 3 also shows that the pH$_{PZC}$ of both activated carbons are acidic (4.97 for AC-H$_3$PO$_4$ and 6.62 for AC-H$_3$BO$_3$). These values concord with Boehm titration results, which show a dominance of acidic groups at the surface of the activated carbons.

3.2. Optimization of process parameters

3.2.1. Effect of solution pH

Changes observed in the adsorption of MB, MV, MO, and IC by AC-H$_3$PO$_4$ and AC-H$_3$BO$_3$ as a function of solution pH are presented in Fig. 4. The figure indicates that as the pH increases, the adsorption capacities for MB and MV increase, while the adsorption capacities for MO and IC decrease. This result may be due to the simultaneous change in surface charge of the adsorbents as well as the dyes functional groups. The pH of zero charge (pH$_{PZC}$) of the adsorbents were found to be 4.97 and 6.62 for AC-H$_3$PO$_4$ and AC-H$_3$BO$_3$, respectively. These values indicate that the adsorbents acquire a positive charge below a pH of 4.97 and 6.62, respectively. At pH values above this point, there is a net negative charge on the cell surface and the ionic state of functional groups such as carboxyl, phosphoryl, sulfhydryl, hydroxyl, and amino. Consequently, the adsorbent–adsorbate interactions for the cationic dyes become progressively significant for higher pH values. We can conclude from this result that the negative surface charge of the activated carbon becomes greater with increasing solution pH. The quantities of dyes adsorbed by AC-H$_3$PO$_4$ are larger than those adsorbed by AC-H$_3$BO$_3$. This difference may be due to the degree of activation of each adsorbent.

3.2.2. Effect of adsorbent dose

Data obtained from the experiments with varying adsorbents concentration are presented in Fig. 5. The figure

Table 3
Chemical groups on the surface of the ACs

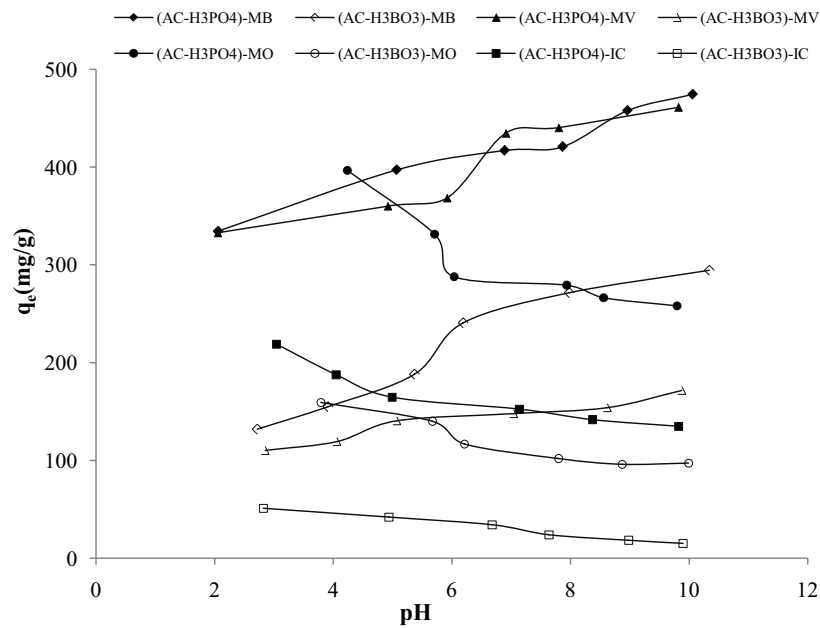| Activated carbon	Surface groups (meq/g)					pH_{PZC}
	Carboxylic	Lactonic	Phenolic	Total acid	Total basic	
CA-H$_3$PO$_4$	0.441	0.494	0.516	1.451	0.399	4.97
CA-H$_3$BO$_3$	0.432	0.496	0.489	1.418	0.367	6.62

Fig. 4. Effect of solution pH on the sorption of dyes onto AC-H$_3$PO$_4$ and AC-H$_3$BO$_3$: C_0 = 500 mg/L, contact time = 120 min, R = 1 g/L, and T = 25°C.

shows that increase in adsorbent dosage of ACs resulted in a   sharp increase in the adsorption yield. The adsorption yield
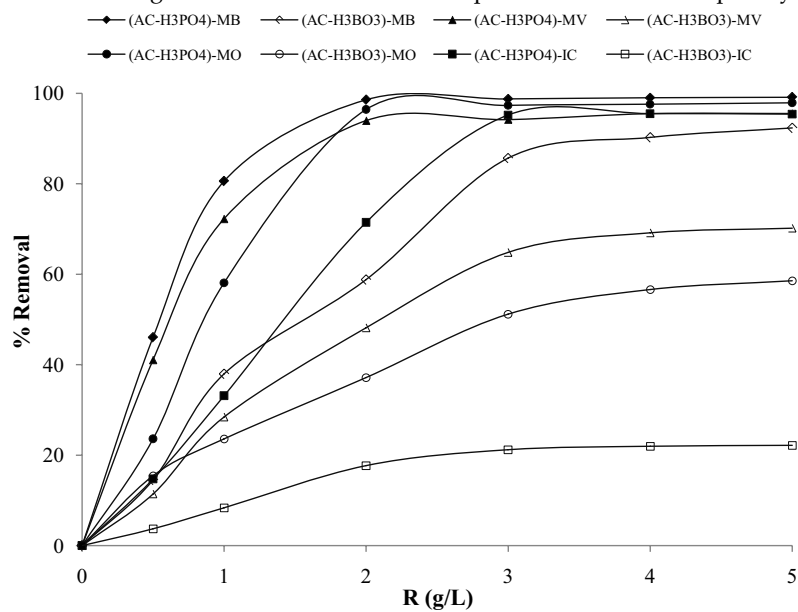

Fig. 5. Effect of adsorbent dosage on the sorption of dyes onto AC-H$_3$PO$_4$ and AC-H$_3$BO$_3$: C_0 = 500 mg/L, contact time = 120 min, initial pH, and T = 25°C.

of MB, MV, and MO was increased more than 90% and just 70% for IC when the adsorbent dosage of AC-H$_3$PO$_4$ reached 2 g/L. The adsorption yield reached 58.78%, 48.13%, 37.15%, and 17.70% for MB, MV, MO, and IC, respectively, when the adsorbent dosage of AC-H$_3$BO$_3$ was 2 g/L. The observed enhancement in adsorption yield with increasing adsorbent concentration could be due to an increase in the number of possible binding sites and surface area of the adsorbents [27].

3.2.3. Effect of contact time

The kinetic parameters, which are supportive of the prediction of adsorption rate and equilibrium time, provide important information for designing and modeling of the adsorption processes. The results of the study of the influence of contact time on the adsorption of dyes onto AC-H$_3$PO$_4$ and AC-H$_3$BO$_3$ are presented in Fig. 6. The figure indicates that the adsorption was rapid during the first period of the process and then the rate of adsorption becomes slower and then after stagnates with the increase in contact time. The equilibration times were found to be 120 min for both activated carbons. In order to characterize the kinetics involved in the process, pseudo-first-order and pseudo-second-order rate equations were proposed and the kinetic data were analyzed based on the regression coefficient (r^2) and the amount of dye adsorbed per unit weight of each adsorbent.

The first-order rate expression of Lagergren based on solid capacity is generally expressed as follows [28]:

$$q = q_e \left(1 - e^{-k_1 t}\right) \tag{3}$$

where q_e and q (both in mg/g) are, respectively, the amounts of dye adsorbed at equilibrium and at any time t (min) and k_1 (1/min) is the rate constant of adsorption.

The pseudo-second-order model proposed by Ho and McKay [29] is based on the assumption that the adsorption follows second-order chemisorption. The pseudo-second-order model can be expressed as:

$$q = \frac{k_2 q_e^2 t}{1 + k_2 q_e t} \tag{4}$$

where k_2 (g/mg min) is the rate constant of pseudo-second-order adsorption.

Parameters of the pseudo-first-order and pseudo-second-order models were estimated with the aid of non-linear regression. The obtained data and the correlation coefficients, r^2, are given in Table 4. Table 4 shows that the calculated equilibrium values (q_{cal}) from the pseudo-second-order model were close to the experimental values (q_{exp}) than the others calculated from the pseudo-first-order kinetic model. Also, the values of the correlation coefficient were closer to 1 in the case of pseudo-second-order than of pseudo-first-order model. This suggests that the adsorption of the dyes could be better described by the pseudo-second-order model. This result provides that the adsorption capacity may be due to the higher driving force making the fast transfer of dye molecules to the surface of the adsorbent particles and the availability of the uncovered surface area and the remaining active sites on the adsorbent.

3.2.4. Effect of initial concentration

Equilibrium adsorption studies determine the capacity of the adsorbent, which can be described by an adsorption isotherm, characterized by certain constants whose values give information on the surface properties, heterogeneity, adsorption intensity, and affinity of the particular adsorbent [30]. Furthermore, it gives information about the distribution
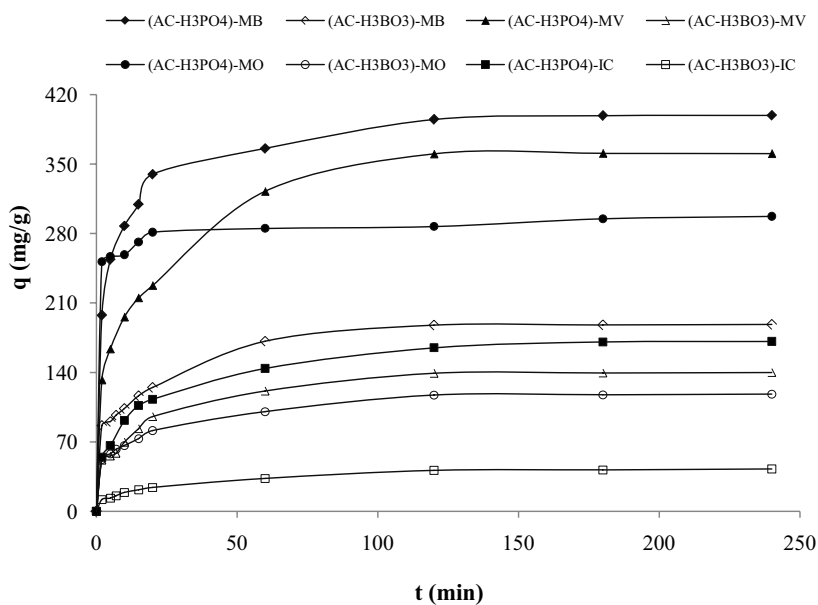

Fig. 6. Kinetics of dyes adsorption by AC-H$_3$PO$_4$ and AC-H$_3$BO$_3$: C_0 = 500 mg/L, R = 1 g/L, initial pH, and temperature = 25°C.

Table 4
Pseudo-first-order and pseudo-second-order kinetic parameters for the sorption dyes by AC-H_3PO_4 and AC-H_3BO_3

Activated carbon	Dye	Pseudo-first-order			Pseudo-second-order			
		q_{cal} (mg/g)	k (1/min)	r^2	q_{exp} (mg/g)	q_{cal} (mg/g)	k (g/mg min)	r^2
AC-H_3PO_4	IC	158.959	0.0812	0.936	164.797	167.888	0.0007	0.977
	MO	279.401	1.1211	0.977	287.085	285.975	0.0095	0.989
	MV	345.038	0.0807	0.897	360.278	366.267	0.0004	0.951
	MB	366.270	0.2438	0.919	395.032	390.930	0.0010	0.982
AC-H_3BO_3	IC	36.839	0.0590	0.934	41.160	43.923	0.0017	0.970
	MO	109.368	0.1083	0.852	117.157	115.887	0.0015	0.931
	MV	133.535	0.0786	0.921	139.076	140.687	0.0008	0.960
	MB	177.902	0.0990	0.847	187.607	187.849	0.0009	0.922

of the solute between the liquid and solid phases at various equilibrium concentrations. The equilibrium adsorption capacity of AC-H_3PO_4 and AC-H_3BO_3 for dyes increased with a rise in initial concentration as shown in Figs. 7 and 8. The figures indicate that high concentration in solution implicates high amount of dye molecules fixed at the surface of the adsorbent. To better understand the adsorption process,

the obtained equilibrium data were analyzed by Langmuir [31] and Freundlich [32] isotherm models.

The calculated isotherm parameters for each model and correlation coefficients estimated by non-linear regressive method are summarized in Table 5. The table indicates that the best fit of experimental data was obtained with the Langmuir model. The values of $r^2 \geq 0.998$ accused the applicability of
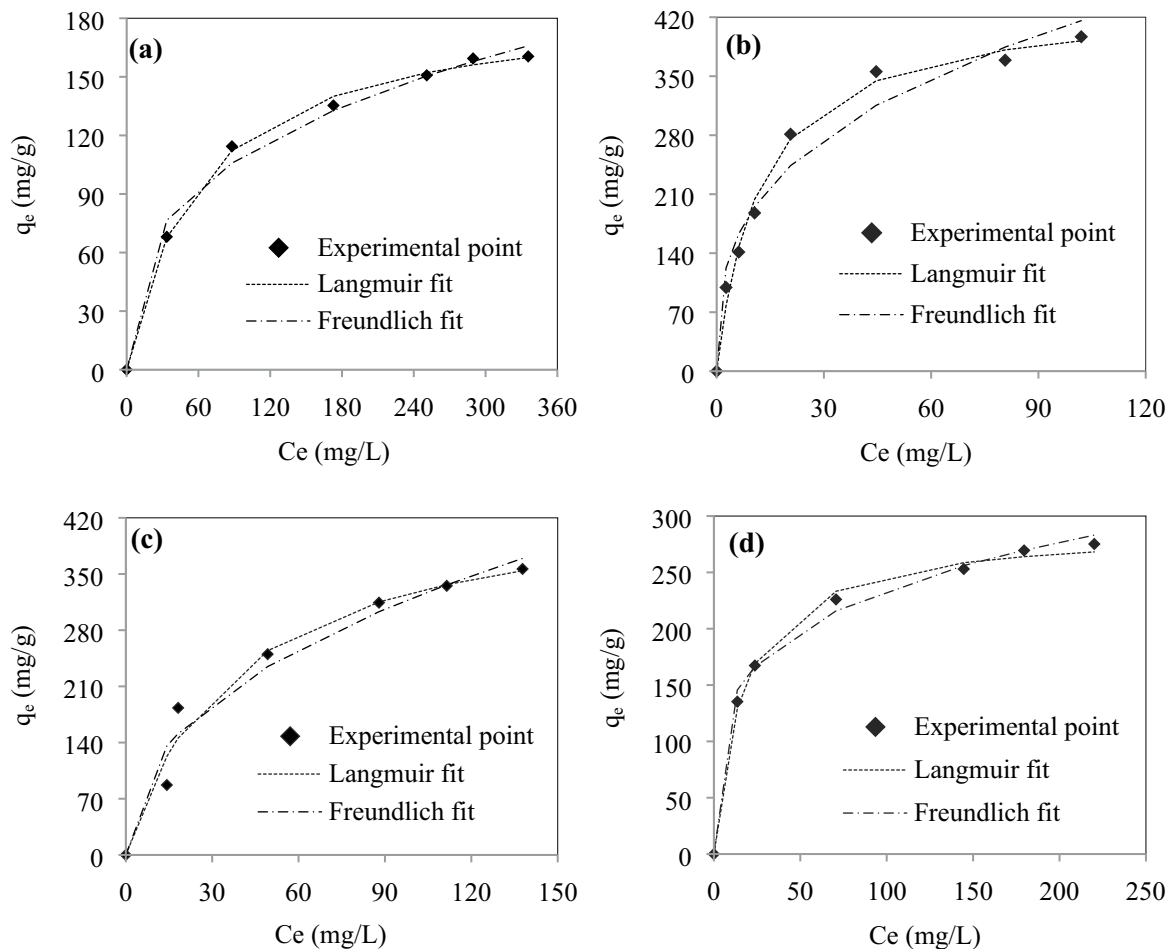

Fig. 7. Experimental points and nonlinear fitted isotherm curves of dyes adsorption by AC-H_3PO_4: (a) IC, (b) MB, (c) MV, and (d) MO.
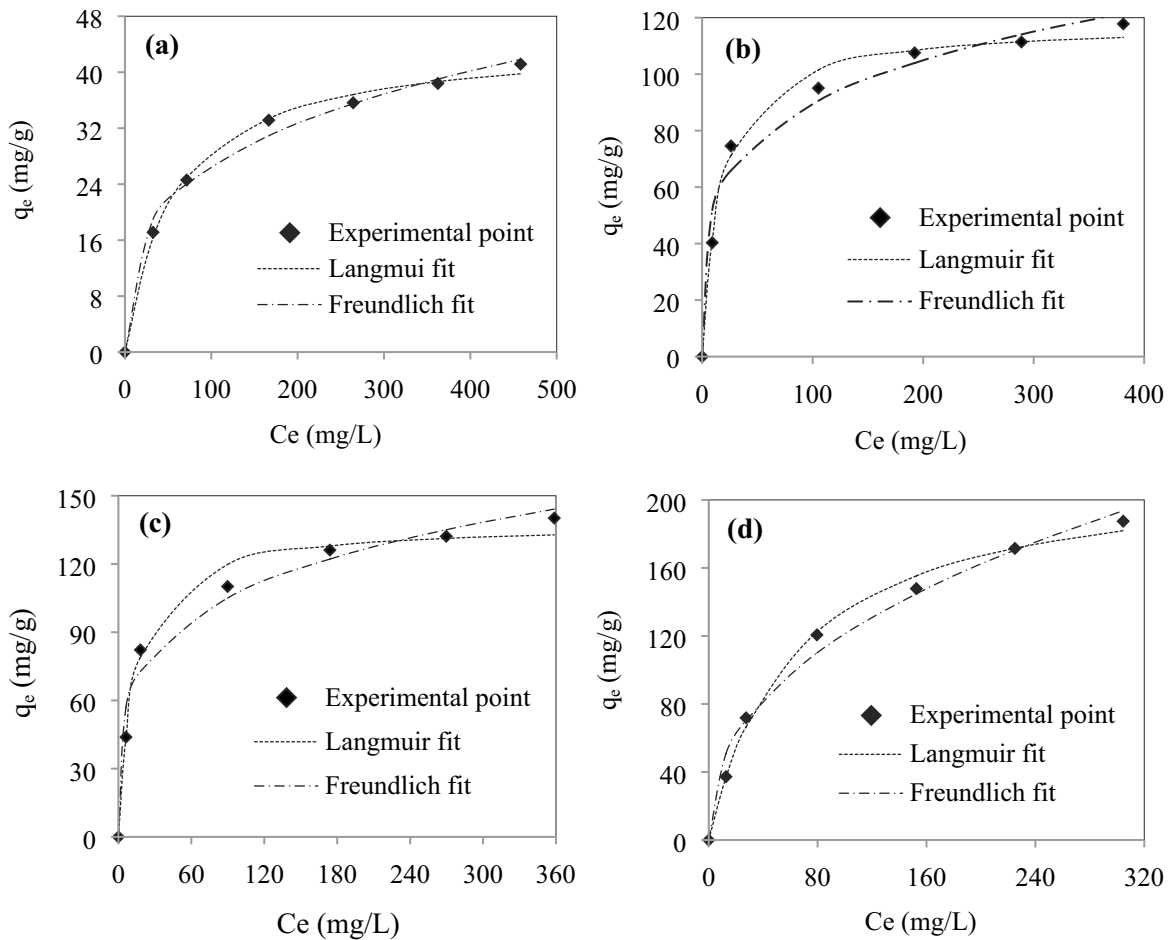
Fig. 8. Experimental points and nonlinear fitted isotherm curves of dyes adsorption by AC-H$_3$BO$_3$ removal of (a) IC, (b) MO, (c) MV, and (d) MB.

Table 5
Isotherm constant parameters and correlation coefficients calculated for the sorption of dyes onto AC-H$_3$PO$_4$ and AC-H$_3$BO$_3$

Isotherm model	Parameters	AC-H$_3$PO$_4$				AC-H$_3$BO$_3$			
		IC	MO	MV	MB	IC	MO	MV	MB
Langmuir	q_m (mg/g)	188.25	288.61	452.58	439.08	44.70	118.10	137.80	219.70
	K_L (L/mg)	0.017	0.06	0.026	0.082	0.018	0.058	0.074	0.016
	r^2	0.998	0.997	0.975	0.993	0.997	0.993	0.99	0.996
Freundlich	n	2.977	4.190	2.266	2.992	3.343	4.379	4.372	2.375
	K_F (mg$^{1-1/n}$/g/ln)	23.515	78.131	42.012	88.628	6.692	31.282	37.535	17.424
	r^2	0.991	0.994	0.964	0.968	0.992	0.977	0.98	0.988

the Langmuir model. The maximum Langmuir monolayer adsorption capacities were 439.08 and 219.70 mg/g for MB, 452.58 and 137.80 mg/g for MV, 288.61 and 118.10 mg/g for MO, and 188.25 and 44.70 mg/g in the case of IC, respectively, for AC-H$_3$PO$_4$ and AC-H$_3$BO$_3$. For the Freundlich model, the correlation coefficients are lower.

Maximum adsorption capacities obtained were compared to the previous records of various adsorbents as summarized in Table 6. It can be observed that experimental data of the present study were found to be higher than those of the most corresponding adsorbents in the literature. The result is due to the nature of functional groups present in the surface of the prepared activated carbons.

3.2.5. Effect of temperature and thermodynamic parameters

The variation of adsorbed quantities of dyes onto AC-H$_3$PO$_4$ and AC-H$_3$BO$_3$ as a function of solution

Table 6
Comparison of adsorption capacities (mg/g) of activated carbons with literatures

Activated carbon	Activating agent	MB	MV	MO	IC	References
Activated coffee ground	HNO_3	–	–	558	–	[14]
Activated *Diplotaxis harra*	H_3PO_4	262.1	–	–	–	[15]
Activated *Glebionis coronaria* L.	H_3PO_4	161.92	–	–	–	[16]
Activated maize corncob	H_3PO_4	271.19	–	–	–	[17]
Activated beetroot seeds	H_3PO_4	74.37	–	–	–	[18]
Activated apricot stones	$H_3PO_4+HNO_3$	–	–	32.25	–	[19]
Phragmites australis activated carbon	H_3PO_4	–	500	217.39	–	[33]
Activated *Camellia sinensis* leaves	H_3PO_4	322.7	–	–	–	[34]
Activated Persian mesquite grain	H_3PO_4	–	–	66.3	–	[35]
Activated prickly pear peels	H_3PO_4	–	–	–	294.1	[36]
Activated white sapote seeds	H_3PO_4	–	–	–	131.6	[36]
Activated broccoli stems	H_3PO_4	–	–	–	312.5	[36]
Activated *Limonia acidissima* shell	H_3PO_4	–	–	–	–	[37]
Posidonia oceanica (L.) dead leaves	$ZnCl_2$	285.7	–	–	–	[38]
Activated *Glebionis coronaria* L.	KOH	284.04	–	–	–	[39]
Activated grapevine rhytidome	H_3PO_4	–	161.3	–	–	[40]
Activated Orange peel	H_3BO_3	149	–	–	–	[41]
Activated *Thapsia transtagana* stems	H_3PO_4	397.54	358.68	287.47	164.57	This study
Activated *Thapsia transtagana* stems	H_3BO_3	188.75	140.76	116.84	41.46	This study

temperature is shown in Fig. 9. A decrease in the removal efficiency was observed with an increase in temperature. From these results, thermodynamic parameters including the change in free energy ($\Delta G°$), enthalpy ($\Delta H°$), and entropy ($\Delta S°$) were used to describe thermodynamic behavior of the adsorption of the dyes. These parameters were calculated by considering a reversible adsorption process. For such equilibrium reactions, K_D, the distribution constant, can be expressed as:

$$K_D = \frac{q_e}{C_e} \tag{5}$$

The Gibbs free energy is:

$$\Delta G° = -RT\ln\left(K_D\right) \tag{6}$$

where R is the universal gas constant (8.314 J mol/K) and T is solution temperature in K.

The enthalpy ($\Delta H°$) and entropy ($\Delta S°$) of adsorption were estimated from the slope and intercept of the plot of $\ln K_D$ vs. $1/T$ yields, respectively.

$$\ln K_D = -\frac{\Delta G°}{RT} = -\frac{\Delta H°}{RT} + \frac{\Delta S°}{R} \tag{7}$$

The thermodynamic parameters calculated from the values of the slopes and the intercepts are reported in Table 7. A negative $\Delta G°$ value indicates that the removal process is spontaneous for MB, MV, and MO adsorption by AC-H_3PO_4. Furthermore, the values of $\Delta G°$ decrease when the temperature rises thus show the increase in the feasibility of the adsorption process at higher temperatures. Then,

the positive values of $\Delta G°$ suggest that adsorption reaction requires energy for the adsorption of IC onto AC-H_3PO_4 and the adsorption of MB, MV, MO, and IC onto AC-H_3BO_3 [42].

The increase in $\Delta G°$ values with an increase in temperature shows a decrease in the feasibility of adsorption at higher temperatures. The values of $\Delta H°$ are negative for all investigated systems and they are lower than 40 kJ/mol which indicates the exothermic physisorption nature of adsorption. Therefore, the adsorption processes were not favorable at higher temperatures. The negative value of $\Delta S°$ for the corresponding temperature interval indicated decreased randomness at the solid-solution interface with the loading of species onto the surface of activated carbons prepared [43]. It also suggested the probability of a favorable adsorption process.

3.3. Desorption and regeneration

Regeneration is an important step to verify the economic feasibility of the adsorption process. The results of desorption tests for MB adsorbed on activated carbons are grouped in Fig. 10. We measured the MB concentration desorbed from the ACs by each of the eluents used H_2O, NaOH, HNO_3, and H_2SO_4. As can be seen in this figure, the desorption percentage of MB is important in the sulfuric acid solution than in the other solutions for activated carbons impregnated with phosphoric acid and boric acid. The desorption percentages of the MB by the H_2SO_4 solution reached 82.89% and 60.41% for AC-H_3PO_4 and AC-H_3BO_3, respectively.

In what follows, we will use the solution of H_2SO_4 (0.1N) for the regeneration of the adsorbents. Fig. 11 gives the percentage of desorption and the adsorption capacity of the MB on the (a) AC-H_3PO_4 and (b) AC-H_3BO_3 regenerated three time.
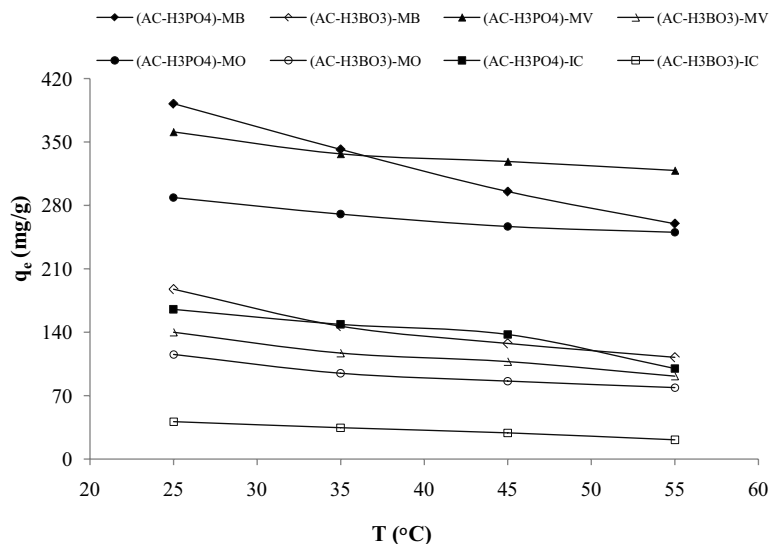
Fig. 9. Effect of temperature on the adsorption of dyes onto AC-H$_3$PO$_4$ and AC-H$_3$BO$_3$: C_0 = 500 mg/L, contact time = 120 min, initial pH, and R = 1 g/L.

Table 7
Thermodynamic parameters calculated for the sorption of dyes by AC-H$_3$PO$_4$ and AC-H$_3$BO$_3$

Activated carbon	Dye	T (K)	K_D	$\Delta G°$ (kJ/mol)	$\Delta H°$ (kJ/mol)	$\Delta S°$ (J/K mol)
AC-H$_3$PO$_4$	IC	298	0.500	1.718	−17.38	−64.04
		308	0.429	2.167		
		318	0.384	2.531		
		328	0.253	3.749		
	MO	298	1.375	−0.788	−9.30	−28.56
		308	1.185	−0.702		
		318	1.061	−0.156		
		328	1.008	−0.022		
	MV	298	2.633	−2.399	−10.33	−26.59
		308	2.088	−1.886		
		318	1.934	−1.746		
		328	1.773	−1.563		
	MB	298	3.793	−3.304	−33.60	−101.60
		308	2.219	−2.042		
		318	1.474	−1.026		
		328	1.102	−0.265		
AC-H$_3$BO$_3$	IC	298	0.090	5.969	−18.38	−81.67
		308	0.075	6.636		
		318	0.062	7.356		
		328	0.045	8.460		
	MO	298	0.304	2.952	−12.52	−51.91
		308	0.237	3.689		
		318	0.210	4.129		
		328	0.190	4.532		
	MV	298	0.392	2.320	−14.44	−56.22
		308	0.307	3.025		
		318	0.276	3.404		
		328	0.225	4.071		
	MB	298	0.606	1.242	−19.46	−69.44
		308	0.419	2.229		
		318	0.346	2.807		
		328	0.292	3.359		

Table 8
Physico-chemical analysis of the textile wastewater

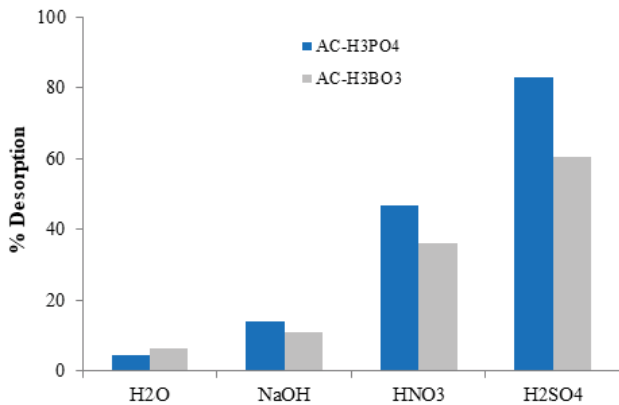| Parameter	Value	Moroccan standards
pH	13.04	5.5–9.0
Temperature, °C	29	30
COD, mg/L	1,984	500
Suspended solids, mg/L	200	150

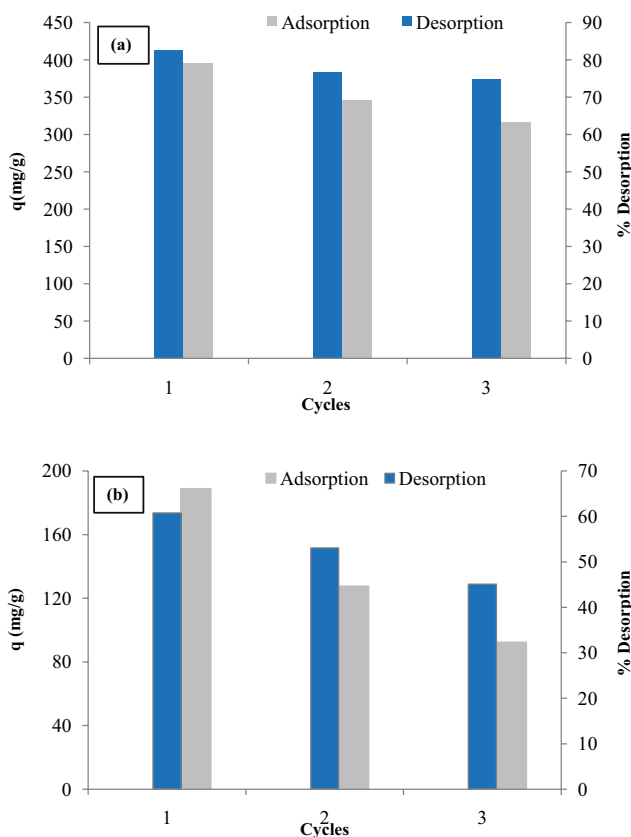Fig. 10. Desorption of MB from ACs by various eluents.

Fig. 11. Efficiency of elimination of AC-H_3PO_4 (a) and AC-H_3BO_3 (b) during three successive cycles of adsorption–desorption tests.

From the results of the regeneration, it was found that the adsorption capacity does not decrease more than 18% and 20% for AC-H_3PO_4 and AC-H_3BO_3, respectively, after three cycles of desorption–adsorption compared to the initial adsorption capacity. This decrease in adsorption capacity may be due to the decomposition or damage caused by an acidic solution at some adsorption sites or functional groups present on the adsorbent surface [44]. So, this regeneration method seems to be effective for the reuse of adsorbents, but it makes sense to do an economic study to study its feasibility and its justification from the economic point of view.

3.4. Application of ACs for the treatment of TWW

3.4.1. Characteristics of TWW

To evaluate the pollution content, sample TWW was characterized and the results were compared with Moroccan wastewater discharge standards established by the ministry of the environment of Morocco [45] as shown in Table 8. The pH of effluent sample appeared to be 13.04. This high value could influence the physico-chemical properties of water, which influence negatively on aquatic life, plants, and humans. This also changes the soil permeability, which influences in polluting underground resources of water. The UV-visible absorption spectrum of TWW was presented in Fig. 12. The spectrum is based on the nature of the pollutants
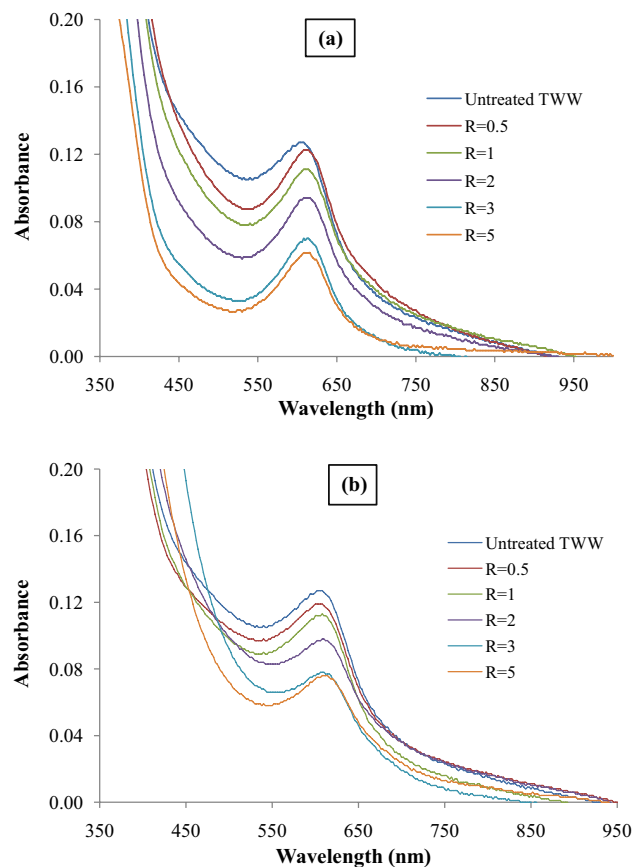

Fig. 12. Variation in UV-visible spectra of TWW at different ACs dosages: (a) AC-H_3PO_4 and (b) AC-H_3BO_3.

existing in the effluent, absorbing the light in a precise wavelength range. It is not easy to determine the principal dyes and substances used in the dying process from UV-visible absorption data, because of the complexity of the TWW. This complexity is partly due to the mixture of the dyes and substances used. The COD value of TWW was 1,984 mg/L, which exceeds the limits authorized by Moroccan standards (500 mg/L). This value is influenced by the presence of oxidizable organic and/or inorganic compounds.

The experiments were carried out in order to reduce the toxicity of the TWW and testing the AC-H_3PO_4 and AC-H_3BO_3 for color and COD removal from effluents generated by this textile industry.

3.4.2. Color removal

The variation in UV-Vis absorption spectra of color removal from wastewater as a function of the dose of AC-H_3PO_4 (a) and AC-H_3BO_3 (b) is shown in Fig. 12. According to the UV-visible absorption spectra, it was found that when the dose of activated carbons used increases the apparent affinity of pollutant adsorbate for the adsorbent increases. This retention is translated by a decrease of the characteristic absorbance to the rejection spectrum after the addition of different masses of each ACs. Measurement of the absorbance, index of the coloration of the rejection, shows that the percentage of the discoloration reaches 50% and 32% with a quantity of 5 g/L for AC-H_3PO_4 and AC-H_3BO_3, respectively.

3.4.3. COD abatement

The effect of the adsorbent dose on the COD removal was evaluated by varying the dosages of each of the adsorbents between 0.5 and 5 g/L. Fig. 13 represent the evolution of the amount of COD retained by different masses of AC-H_3PO_4 and AC-H_3BO_3. This figure shows that the amount of COD decreases as the dose of activated carbons increases and reaches a plateau when adding a mass of 2 g/L for AC-H_3PO_4 and a mass of 3 g/L for AC-H_3BO_3, these values are the optimal mass to reduce the COD value. AC-H_3PO_4 activated carbon gave the best result with maximum retention of 73.21%. The value of the COD before the treatment is 1,984 mg/L, this value presents toxicity for the environment, a dose of 2 g/L is able to reduce the COD of the rejection to respect the Moroccan laws in force.

3.4.4. Effect of pH on COD removal

The influence of pH on COD abatement by AC-H_3PO_4 and AC-H_3BO_3 at various pH values is shown in Fig. 14. From this figure, it can be noted that there is a reduction in the percentage of COD abatement for all pH values. The COD abatement percentages reached 69.56% and 56.20% were found at pH equal to 4 for AC-H_3PO_4 and AC-H_3BO_3, respectively.

4. Conclusion

This study examined the potential of two activated carbons prepared from TTS by phosphoric acid and boric acid
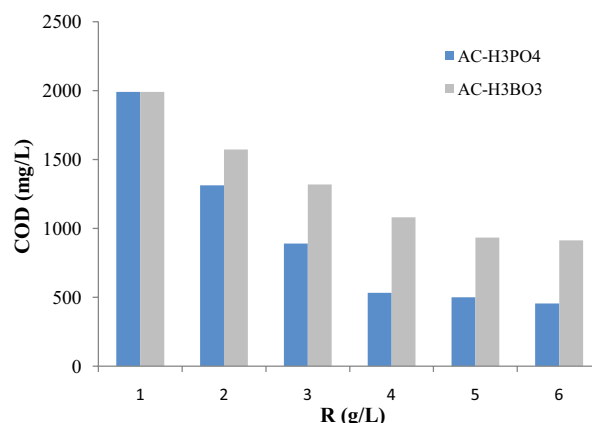
Fig. 13. Variation in the amount of COD as a function of the added dose of ACs.
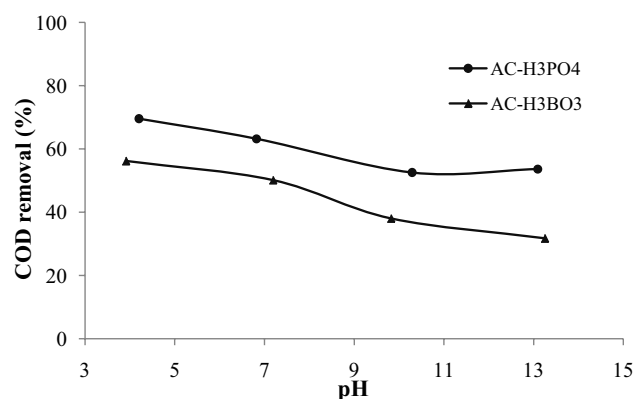
Fig. 14. Effect of pH on COD removal by 1 g/L of ACs.

and their application to the removal of cationic and anionic dyes from aqueous solution. Various adsorption parameters such as contact time, initial dye concentration, adsorbent dose, initial solution pH, and temperature for the removal of dyes by AC-H_3PO_4 and AC-H_3BO_3 were optimized. The adsorption data conformed well Langmuir isotherm, which indicated that the adsorption sites on the surface of adsorbent are energetically homogeneous. The adsorption capacities, for AC-H_3PO_4 were found to be higher than those for AC-H_3BO_3. The kinetic data fitted well pseudo-second-order. The adsorption of the dyes onto activated carbons prepared was exothermic in nature. The reaction was accompanied by a decrease in entropy. The results of the regeneration tests showed that the adsorption capacity does not decrease more than 18% and 20% for AC-H_3PO_4 and AC-H_3BO_3, respectively, after three desorption–adsorption cycles.

The optimum pH value for COD reduction was found near 4. In this condition, the percentage of COD abatement reached 69.56% and 56.20% for AC-H_3PO_4 and AC-H_3BO_3, respectively. Also, the AC-H_3PO_4 gave relatively the best result in COD removal (73.21%) compared to the AC-H_3BO_3. Finally, the present studies showed that activated TTS is a promising adsorbent for the discoloration of effluents containing dyes.

References

[1]   M.O. Awaleh, Y.D. Soubaneh, Waste water treatment in chemical industries: the concept and current technologies, Hydrol. Current Res., 5 (2014).

[2]   C. Allègre, P. Moulin, M. Maisseu, F. Charbit, Treatment and reuse of reactive dyeing effluents, J. Membr. Sci., 269 (2006) 15–34.

[3]   G.L. Dotto, J.M. Moura, T.R.S. Cadaval, L.A.A. Pinto, Application of chitosan films for the removal of food dyes from aqueous solutions by adsorption, Chem. Eng. J., 214 (2013) 8–16.

[4]   M.M. Martorell, H.F. Pajot, L.I.C. de Figueroa, Biological degradation of Reactive Black 5 dye by yeast *Trichosporon akiyoshidainum*, J. Environ. Chem. Eng., 5 (2017) 5987–5993.

[5]   E. do Vale-Júnior, D.R. da Silva, A.S. Fajardo, C.A. Martínez-Huitle, Treatment of an azo dye effluent by peroxi-coagulation and its comparison to traditional electrochemical advanced processes, Chemosphere, 204 (2018) 548–555.

[6]   Y. Liu, W. Zhu, K. Guan, C. Peng, J. Wu, Freeze-casting of alumina ultra-filtration membranes with good performance for anionic dye separation, Ceram. Int., 44 (2018) 11901–11904.

[7]   A. Aouni, C. Fersi, M. Dhahbi, Performance evaluation of direct nanofiltration process to fouling by treating rinsing-bath effluents for water reuse, Desal. Water Treat., 52 (2014) 1770–1785.

[8]   P. Kariyajjanavar, J. Narayana, Y. Arthoba Nayaka, Degradation of textile dye C.I. Vat Black 27 by electrochemical method by using carbon electrodes, J. Environ. Chem. Eng., 1 (2013) 975–980.

[9]   F. Gholami-Borujeni, K. Naddafi, F. Nejatzade-Barandozi, Application of catalytic ozonation in treatment of dye from aquatic solutions, Desal. Water Treat., 51 (2013) 6545–6551.

[10] A. Elhalil, H. Tounsadi, R. Elmoubarki, F.Z. Mahjoubi, M. Farnane, M. Sadiq, M. Abdennouri, S. Qourzal, N. Barka, Factorial experimental design for the optimization of catalytic degradation of malachite green dye in aqueous solution by Fenton process, Water Resour. Ind., 15 (2016) 41–48.

[11] C. Yin, M. Aroua, W. Daud, Review of modifications of activated carbon for enhancing contaminant uptakes from aqueous solutions, Sep. Purif. Technol., 52 (2007) 403–415.

[12] K.M. Smith, G.D. Fowler, S. Pullket, N.J.D. Graham, Sewage sludge-based adsorbents: a review of their production, properties and use in water treatment applications, Water Res., 43 (2009) 2569–2594.

[13] V.M. Monsalvo, A.F. Mohedano, J.J. Rodriguez, Adsorption of 4-chlorophenolby inexpensive sewage sludge-based adsorbents, Chem. Eng. Res. Des., 90 (2012) 1807–1814.

[14] S. Rattanapan, J. Srikram, P. Kongsune, Adsorption of methyl orange on coffee grounds activated carbon, Energy Procedia, 138 (2017) 949–954.

[15] H. Tounsadi, A. Khalidi, M. Abdennouri, N. Barka, Activated carbon from *Diplotaxis Harra* biomass: optimization of preparation conditions and heavy metal removal, J. Taiwan Inst. Chem. Eng., 59 (2016) 348–358.

[16] H. Tounsadi, A. Khalidi, A. Machrouhi, M. Farnane, R. Elmoubarki, A. Elhalil, M. Sadiq, N. Barka, Highly efficient activated carbon from *Glebionis coronaria* L. biomass: optimization of preparation conditions and heavy metals removal using experimental design approach, J. Environ. Chem. Eng., 4 (2016) 4549–4564.

[17] M. Farnane, H. Tounsadi, A. Machrouhi, A. Elhalil, F.Z. Mahjoubi, M. Sadiq, M. Abdennouri, S. Qourzal, N. Barka, Dye removal from aqueous solution by raw maize corncob and H_3PO_4 activated maize corncob, J. Water Reuse Desal., 8 (2018) 214–224.

[18] A. Machrouhi, M. Farnane, A. Elhalil, R. Elmoubarki, M. Abdennouri, S. Qourzal, H. Tounsadi, N. Barka, Effectiveness of beetroot seeds and H_3PO_4 activated beetroot seeds for the removal of dyes from aqueous solutions, J. Water Reuse Desal., 8 (2018) 522–531.

[19] C. Djilani, R. Zaghdoudi, F. Djazi, B. Bouchekima, A. Lallam, A. Modarressi, M. Rogalski, Adsorption of dyes on activated carbon prepared from apricot stones and commercial activated carbon, J. Taiwan Inst. Chem. Eng., 53 (2015) 112–121.

[20] M.F. Machado, C.P. Bergmann, T.H.M. Fernandes, E.C. Lima, B. Royer, T. Calvete, S.B. Fagan, Adsorption of Reactive Red M-2BE dye from water solutions by multi-walled carbon nanotubes and activated carbon, J. Hazard. Mater., 192 (2011) 1122–1131.

[21] C.S. Castro, M.C. Guerreiro, L.C.A. Oliveira, M. Goncalves, A.S. Anastacio, M. Nazzaro, Iron oxide dispersed over activated carbon: support influence on the oxidation of the model molecule methylene blue, Appl. Catal., A, 367 (2009) 53–58.

[22] S. Sadaf, H.N. Bhatti, Batch and fixed bed column studies for the removal of Indosol Yellow BG dye by peanut hush, J. Taiwan Inst. Chem. Eng., 45 (2014) 541–553.

[23] H.P. Boehm, E. Diehl, W. Heck, R. Sappok, Surface oxides of carbon, Angew. Chem. Int. Ed., 3 (1964) 669–677.

[24] J.S. Noh, J.A. Schwarz, Estimation of the point of zero charge of simple oxides by mass titration, J. Colloid Interface Sci., 130 (1989) 157–164.

[25] K. Kinoshita, Carbon, Electrochemical and Physicochemical Properties, Wiley, New York, NY, 1988.

[26] M.R.H. Mas Haris, K. Sathasivam, The removal of methyl red from aqueous solutions using banana pseudo stem fibers, Am. J. Appl. Sci., 6 (2009) 1690–1700.

[27] I. Bakas, K. Elatmani, S. Qourzal, N. Barka, A. Assabbane, Y. Ait-Ichou, A comparative adsorption for the removal of *p*-cresol from aqueous solution onto granular activated charcoal and granular activated alumina, J. Mater. Environ. Sci., 5 (2014) 675–682.

[28] S. Lagergren, About the theorie of so-called adsorption of soluble substance, Kungl. Sven. Vetenskapsakad. Handl., 24 (1898) 1–39.

[29] Y.S. Ho, G. Mckay, The kinetics of sorption of basic dyes from aqueous solution by sphagnum moss peat, Can. J. Chem. Eng., 76 (1998) 822–827.

[30] R. Malik, S. Dahiya, S. lata, An experimental and quantum chemical study of removal of utmostly quantified heavy metals in wastewater using coconut husk: a novel approach to mechanism, Int. J. Biol. Macromol., 98 (2017) 139–149.

[31] I. Langmuir, The constitution and fundamental properties of solids and liquids. Part I. Solids, J. Am. Chem. Soc., 38 (1916) 2221–2295.

[32] H. Freundlich, W. Heller, The Adsorption of cis- and trans-Azobenzene, J. Am. Chem. Soc., 61 (1939) 2228–2230.

[33] S. Chen, J. Zhang, C. Zhang, Q. Yue, Y. Li, C. Li, Equilibrium and kinetic studies of methyl orange and methyl violet adsorption on activated carbon derived from *Phragmites australis*, Desalination, 252 (2010) 149–156.

[34] T. Mahmood, R. Ali, A. Naeem, M. Hamayun, M. Aslam, Potential of used *Camellia sinensis* leaves as precursor for activated carbon preparation by chemical activation with H_3PO_4; optimization using response surface methodology, Process Saf. Environ. Prot., 109 (2017) 548–563.

[35] E.G. Lemrask, S. Sharafinia, M.A. Mohammadi, New activated carbon from persian mesquite grain as an excellent adsorbent, Phys. Chem. Res., 5 (2017) 81–98.

[36] A. Pelaez-Cid, A. Herrera-Gonzalez, M. Salazar-Villanueva, A. Bautista-Hernandez, Elimination of textile dyes using activated carbons prepared from vegetable residues and their characterization, J. Environ. Manage., 181 (2016) 269–278.

[37] S. Das, S. Mishra, Box-Behnken statistical design to optimize preparation of activated carbon from *Limonia acidissima* shell with desirability approach, J. Environ. Chem. Eng., 5 (2017) 588–600.

[38] M.U. Dural, L. Cavas, S.K. Papageorgiou, F.K. Katsaros, Methylene blue adsorption on activated carbon prepared from *Posidonia oceanica* (L.) dead leaves: kinetics and equilibrium studies, Chem. Eng. J., 168 (2011) 77–85.

[39] H. Tounsadi, A. Khalidi, M. Farnane, M. Abdennouri, N. Barka, Experimental design for the optimization of preparation conditions of highly efficient activated carbon from *Glebionis*

Coronaria L. and heavy metals removal ability, Process Saf. Environ. Prot., 102 (2016) 710–723.

[40] M. Hejazifar, S. Azizian, H. Sarikhani, Q. Li, D. Zhao, Microwave assisted preparation of efficient activated carbon from grapevine rhytidome for the removal of methyl violet from aqueous solution, J. Anal. Appl. Pyrolysis, 92 (2011) 258–266.

[41] C. Akmil-Başar, E. Köseoğlu, Y. Önal, Utilization potential lignocellulosic waste biomass to produce carbon support by using new activation reagent (H_3BO_3 and $SrCl_2$): structural and adsorptive properties, J. Part. Sci. Technol., 34 (2016) 526–532.

[42] M.E. Mahmoud, G.M. Nabil, Nano zirconium silicate coated manganese dioxide nanoparticles: microwave-assisted synthesis, process optimization, adsorption isotherm, kinetic study and thermodynamic parameters for removal of 4-nitrophenol, J. Mol. Liq., 240 (2017) 280–290.

[43] M.A.A. Khalek, G.A. Mahmoud, E.M. Shoukry, M. Amin, A.H. Abdulghany, Adsorptive removal of nitrate ions from aqueous solution using modified biodegradable-based hydrogel, Desal. Water Treat., 155 (2019) 390–401.

[44] S. Hosseini, M.A. Khan, M.R. Malekbala, W. Cheah, T.S.Y. Choong, Carbon coated monolith, a mesoporous material for the removal of methyl orange from aqueous phase: adsorption and desorption studies, Chem. Eng. J., 171 (2011) 1124–1131.

[45] Ministry of the Environment of Morocco, Moroccan Standards, Morocco's Official Bulletin, No. 5062, Rabat, 2002.